



# The GLONASS-M satellite yaw-attitude model

F. Dilssner\*, T. Springer, G. Gienger, J. Dow

*European Space Operations Centre (ESOC), Robert-Bosch-Strasse 5, DE-64293 Darmstadt, Germany*

Received 9 June 2010; received in revised form 6 September 2010; accepted 7 September 2010

## Abstract

The proper modeling of the satellites' yaw-attitude is a prerequisite for high-precision Global Navigation Satellite System (GNSS) positioning and poses a particular challenge during periods when the satellite orbital planes are partially eclipsed. Whereas a lot of effort has been put in to examine the yaw-attitude control of GPS satellites that are in eclipsing orbits, hardly anything is known about the yaw-attitude behavior of eclipsing GLONASS-M satellites. However, systematic variations of the carrier phase observation residuals in the vicinity of the orbit's noon and midnight points of up to  $\pm 27$  cm indicate significant attitude-related modeling issues. In order to explore the GLONASS-M attitude laws during eclipse seasons, we have studied the evolution of the horizontal satellite antenna offset estimates during orbit noon and orbit midnight using a technique that we refer to as "reverse kinematic precise point positioning". In this approach, we keep all relevant global geodetic parameters fixed and estimate the satellite clock and antenna phase center positions epoch-by-epoch using 30-second observation and clock data from a global multi-GNSS ground station network. The estimated horizontal antenna phase center offsets implicitly provide the spacecraft's yaw-attitude. The insights gained from studying the yaw angle behavior have led to the development of the very first yaw-attitude model for eclipsing GLONASS-M satellites. The derived yaw-attitude model proves to be much better than the nominal yaw-attitude model commonly being used by today's GLONASS-capable GNSS software packages as it reduces the observation residuals of eclipsing satellites down to the normal level of non-eclipsing satellites and thereby prevents a multitude of measurements from being incorrectly identified as outliers. It facilitates continuous satellite clock estimation during eclipse and improves in particular the results of kinematic precise point positioning of ground-based receivers.

© 2010 COSPAR. Published by Elsevier Ltd. All rights reserved.

*Keywords:* Yaw-attitude; GLONASS-M; Eclipse season; Kinematic precise point positioning

## 1. Introduction

In order to achieve high-precision GNSS results it is vitally important to know the exact orientation of the transmitting satellites with respect to a specific coordinate system. To describe the spacecraft's orientation, also referred to as its attitude, usually a body-fixed reference system (BFS) is defined. The origin of this BFS coincides with the satellite's center of mass (CM). The  $y$ -axis points along the nominal rotation axis of the solar panel, the  $z$ -axis points along the navigation antenna boresight and the  $x$ -axis completes the orthogonal right-hand system. The attitude of the GNSS satellite is dictated by two con-

straints. First, the navigation antenna along the  $z$ -axis needs to be pointed continuously toward geocenter in order to ensure an adequate signal reception on the Earth's surface (or in the Earth-near space) and second, the surface of the solar panel has to be orientated perpendicular to the Sun–satellite direction at all times in order to optimize the on-board power supply. To meet these two requirements the GNSS satellite has to rotate permanently keeping its body-fixed  $x$ -axis and  $z$ -axis always in the Earth–satellite–Sun plane. This is achieved by rotations along the  $y$ -axis ("pitch-axis") and the  $z$ -axis ("yaw-axis") commonly provided by momentum wheels. The Sun's position is monitored by the attitude control system (ACS) solar sensors. When the satellites' view of the Sun is obstructed by the Earth, however, the solar sensors' signal does not represent the actual yaw-attitude anymore. The proper modeling of

\* Corresponding author.

*E-mail address:* [florian.dilssner@esa.int](mailto:florian.dilssner@esa.int) (F. Dilssner).

the spacecrafts' yaw-motion during eclipse season is further complicated by limited hardware yaw rates.

Whereas a lot of effort has been put in to understand the yaw-attitude control of Global Positioning System (GPS) satellites that are in eclipsing orbits, hardly anything in this field is known about the second spacecraft-generation of the Russian Global Navigation Satellite System (Global'naya Navigatsionnaya Sputnikovaya Sistema) – the GLONASS-M satellites. The yaw-attitude laws of the GLONASS-M space vehicles during eclipse season, however, need to be well-understood as deficiencies in the yaw-attitude model generally lead to measurement correction errors and dynamic orbit errors (Bar-Sever, 1994). Measurement correction errors result from an improper modeling of the antenna phase center location and the antenna phase wind-up effect (Wu et al., 1993). The largest attitude-related antenna phase center correction errors in GNSS have to be expected for the GLONASS-M satellites as their nominal horizontal antenna phase center eccentricity with respect to the  $z$ -rotation axis ( $\tilde{x}_0 = -54.5$  cm,  $\tilde{y}_0 = 0.0$  cm; Mitrikas, 2005) is extremely large. By way of comparison, the nominal horizontal antenna phase center eccentricity of the GPS Block II/IIA spacecraft ( $\tilde{x}_0 = 27.9$  cm,  $\tilde{y}_0 = 0.0$  cm) is about half of this size and the GPS satellites of the Block IIR/IIR-M generation do not exhibit any horizontal phase center offsets at all.<sup>1</sup> An erroneous phase wind-up correction due to yaw-attitude mismodeling is generally less critical, at least for geodetic applications, even though a full turn around the satellite's  $z$ -axis may additionally falsify the carrier phase observations in the order of one wavelength (=10.7 cm for the ionosphere-free linear combination). However, as long as the pseudo-range observations are down-weighted sufficiently, an attitude-related phase wind-up error is either absorbed by the satellite clock parameters or eliminated by double differencing. Dynamic orbit errors may arise due to improper modeling of the solar pressure force which is a strong function of the attitude as well.

In this paper, we introduce the very first yaw-attitude model for GLONASS-M satellites traveling in eclipsing orbits around the Earth. The paper is organized as follows. Section 2 includes background information on the yaw-attitude difficulties arising during the eclipse season and gives a short overview of the yaw-attitude behavior of other GNSS satellites. Section 3 briefly describes the processing strategy which has been applied to explore the yaw-attitude laws of the GLONASS-M spacecraft. The insights gained from the analysis are given in Section 4, followed by a mathematical description of the yaw-attitude model in Section 5. In Section 6, we validate the performance of the proposed model against the nominal yaw-attitude standard model commonly being used by today's

GLONASS-capable GNSS software packages. Finally, we summarize the key results in Section 7.

## 2. Basic relations

### 2.1. Definition of the nominal yaw angle and its rate

The nominal yaw angle  $\psi_n$  is defined as the angle between the nominal body-fixed  $x$ -axis and the instantaneous direction of the spacecraft's velocity ("along-track") vector. For the sake of simplicity, we consistently use here the axis conventions of the GPS Block II/IIA satellites meaning that the  $x$ -axis is required to point positive toward the hemisphere containing the Sun. According to this definition, the nominal yaw angle can be computed as:

$$\psi_n = \text{ATAN2}(-\tan \beta, \sin \mu), \quad (1)$$

with  $\beta$  being the elevation of the Sun above the particular orbital plane and  $\mu$  being the geocentric orbit angle between satellite and orbit midnight, measured in the direction of the spacecraft's motion (Bar-Sever, 1996).  $\text{ATAN2}(a,b)$  is the usual FORTRAN function of  $\arctan(a/b)$  giving unambiguous results in the range of  $[-180^\circ, +180^\circ]$ . The sign of the yaw angle  $\psi_n$  is always opposite to that of the  $\beta$ -angle, which in turn is defined to be positive if the Earth–Sun vector forms an acute angle with the satellite angular momentum vector and negative otherwise (Fig. 1).

The nominal theoretical yaw rate of the spacecraft can be approximated by:

$$\dot{\psi}_n = \dot{\mu} \tan \beta \cos \mu / (\sin^2 \mu + \tan^2 \beta), \quad (2)$$

with  $\dot{\mu}$  being the average orbital angular velocity (Bar-Sever, 1996). Twice per revolution,  $\dot{\psi}_n(\mu)$  reaches a local maximum – firstly, if the spacecraft is at the closest point of the Sun ( $\mu = 180^\circ$ ) and secondly, if it is farthest away from the Sun ( $\mu = 0^\circ$ ). These points on the satellite's trajectory are called "orbit noon" and "orbit midnight", respectively. The nominal yaw rate in the vicinity of orbit noon and orbit midnight requires high spacecraft yaw rates, particularly when the Sun is near the orbital plane and the  $\beta$ -angle is small. As the elevation  $\beta$  of the Sun equals  $0^\circ$ , the nominal yaw rate at the orbit's noon and midnight points becomes infinite and a near instantaneous  $180^\circ$  yaw-flip is theoretically required.

### 2.2. Relationship between the satellite's antenna phase center and its yaw angle

The point of reference for describing the motion of a satellite is the CM of the spacecraft. GNSS measurements, however, always refer to the electrical phase center of the transmitting antenna, which is neither a physical nor a stable point in space. The variation of the antenna's phase center location as a function of the direction of the outgoing signal on a specific carrier frequency is what we call the phase center variation (PCV). The mean phase center is

<sup>1</sup> The 12 next-generation GPS Block IIF space vehicles will also exhibit a significant horizontal antenna phase center eccentricity ( $\tilde{x}_0 = 39.4$  cm,  $\tilde{y}_0 = 0.0$  cm; Choi, 2002; Dilssner, 2010).

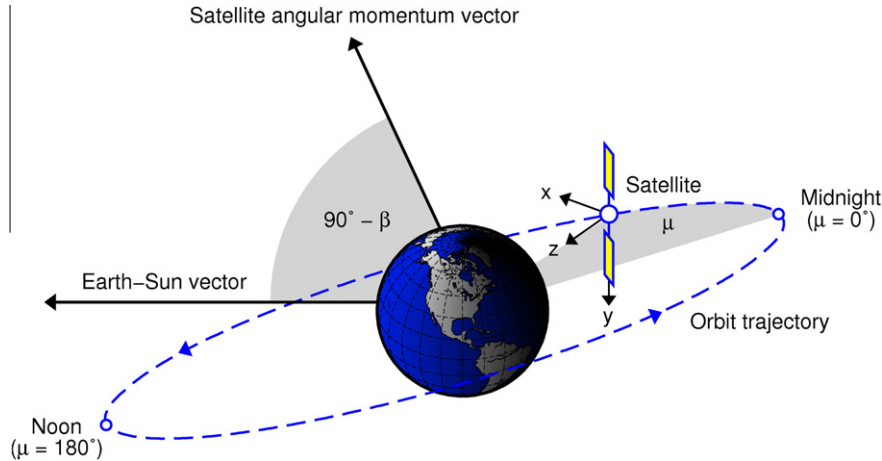


Fig. 1. Definition of the elevation  $\beta$  of the Sun above the orbital plane and the spacecraft's geocentric orbit angle  $\mu$ . “Midnight” denotes the farthest point of the orbit from the Sun whereas “noon” denotes the closest point.

defined as the point for which the phase of the outgoing signal shows the smallest (in the sense of least-squares) PCV. The difference between the position of the mean phase center and the CM is what we call the phase center offset (PCO). PCOs and PCVs must be precisely known with respect to the BFS so that we can tie the GNSS measurements consistently to the satellite's CM (see, e.g., Dilssner et al., 2010).

The phase center correction accounting for the satellite antenna offset is defined by the scalar product of the PCO vector  $\mathbf{r} = (x_0, y_0, z_0)$  and the unit vector  $\mathbf{e} = (\sin \alpha \sin \eta, \cos \alpha \sin \eta, \cos \eta)$  pointing from the satellite to the ground station and can be expressed as follows:

$$\Delta\phi(\alpha, \eta) = x_0 \sin \alpha \sin \eta + y_0 \cos \alpha \sin \eta + z_0 \cos \eta, \quad (3)$$

whereas  $\alpha$  denotes the azimuth and  $\eta$  the nadir-angle under which the particular ground station is seen from the satellite. The azimuth  $\alpha$  is chosen to count clockwise from the  $y$ -axis toward the  $x$ -axis when looking in the direction of the negative  $z$ -axis (Rothacher and Schmid, 2006).

Instead of keeping the satellite antenna PCOs fixed and using Eq. (3) as a priori measurement correction, the relationship can be exploited vice-versa to determine the PCOs from measurements of a global station network. Estimating the horizontal PCO components  $(x_0, y_0)$ , however, requires an exact knowledge of the actual yaw angle at each point in time. The same applies, incidentally, for possible azimuth-dependent PCVs. An inaccurate yaw angle at a certain epoch  $t$  would systematically falsify all azimuth-angles belonging to that epoch which, in turn, would have a certain impact on the horizontal PCO estimates. The effect can be interpreted geometrically as a rotation around the  $z$ -axis. The relationship between mismodeled PCOs  $(x_0, y_0)$  and nominal PCOs  $(\tilde{x}_0, \tilde{y}_0)$  can generally be expressed as follows:

$$\begin{aligned} x_0(t) &= \tilde{x}_0 \cos \Delta\psi(t) - \tilde{y}_0 \sin \Delta\psi(t), \\ y_0(t) &= \tilde{x}_0 \sin \Delta\psi(t) + \tilde{y}_0 \cos \Delta\psi(t), \end{aligned} \quad (4)$$

with  $\Delta\psi(t)$  being the unknown yaw bias at the epoch  $t$ . Since the nominal mean antenna phase center of the GLONASS-M or the GPS Block II/IIA satellites is located within the  $xz$ -plane ( $\tilde{y}_0 = 0.0$  cm), we may simplify the above formulas. This yields:

$$x_0(t)/\tilde{x}_0 = \cos \Delta\psi(t), \quad y_0(t)/\tilde{x}_0 = \sin \Delta\psi(t). \quad (5)$$

Obviously, the yaw bias  $\Delta\psi$  can now be calculated from epoch-wise estimates for the horizontal PCOs  $(x_0, y_0)$ :

$$\Delta\psi(t) = \text{ATAN2}[y_0(t)/\tilde{x}_0, x_0(t)/\tilde{x}_0]. \quad (6)$$

Note that for  $\tilde{x}_0 > 0$  (GPS) this simplifies to:

$$\Delta\psi(t) = \text{ATAN2}[y_0(t), x_0(t)], \quad (7)$$

whereas for  $\tilde{x}_0 < 0$  (GLONASS) we obtain:

$$\Delta\psi(t) = \text{ATAN2}[-y_0(t), -x_0(t)]. \quad (8)$$

Alternatively, the yaw bias  $\Delta\psi$  can be estimated directly rather than deriving it from the horizontal PCO parameters. This may be beneficial in terms of processing power and memory resources as only half the number of additional parameters have to be set up. Substituting Eq. (5) into Eq. (3) yields the required observation equation:

$$\Delta\phi(\Delta\psi) = \tilde{x}_0 \sin(\alpha + \Delta\psi) \sin \eta + \tilde{z}_0 \cos \eta, \quad (9)$$

with  $\Delta\psi$  being the unknown parameter to be solved for. Absolute estimates for the actual yaw angles can finally be obtained from:

$$\psi(t) = \psi_0(t) + \Delta\psi(t), \quad (10)$$

whereas  $\psi_0$  denotes the underlying a priori yaw angle.

Error propagation shows that the precision of the estimated yaw angle  $\psi$  is inherently governed by the distance between horizontal phase center position and CM: The larger the distance, the better the precision. Viewed in this light, a large horizontal satellite antenna offset does not always have to be a disadvantage. Comparisons between nominal and estimated yaw angles done for several non-eclipsing GLONASS-M satellites indicate RMS values no

worse than  $\pm 3^\circ$ . Needless to say that the approach cannot be applied to GNSS satellites having no horizontal antenna phase center eccentricities (e.g., GPS Block IIR/IIR-M satellites).

### 2.3. Eclipse season

The elevation  $\beta$  of the Sun with respect to the particular GNSS satellite orbital plane varies while the Earth's revolves around the Sun. Every six months, during the four to eight weeks of the “eclipse season” of the orbital plane, the  $\beta$ -angle is so small that once per revolution each satellite of the orbital plane passes through the shadow of the Earth for a short period of time. In the case of the GLONASS satellite constellation, only one orbital plane is partially eclipsed at the same time as the evolution of the  $\beta$ -angle with respect to the three orbital planes between January 2008 and December 2009 indicates (Fig. 2).

The Earth's shadow is divided into two cone-shaped regions, the umbra and the penumbra (Fig. 3). The completely dark portion of the shadow cast by the Earth during the eclipse is called umbra. The region in which only a portion of the sunlight is obscured by the Earth is called penumbra. The Earth–spacecraft–Sun angle  $\epsilon_0$  of a GLONASS-M satellite at the entrance and the exit of the umbra (penumbra) is  $\pm 14.20^\circ$  ( $\pm 14.73^\circ$ ). A GLONASS-M satellite traveling with a mean orbital angular velocity of  $\dot{\mu} = 0.00888^\circ/\text{s}$  around the Earth may therefore need up to around 53 min for its passage through the umbra.

### 2.4. Yaw-attitude during eclipse season

#### 2.4.1. GPS satellites

GPS satellites are able to maintain their nominal orientation most of the time. During eclipse seasons, however, significant deviations between actual and nominal yaw-attitude may occur. Whenever a GPS Block IIR satellite reaches a certain point in the vicinity of orbit noon or orbit midnight and the elevation  $\beta$  of the Sun is below  $2.4^\circ$ , it cannot keep up anymore with the rapidly changing nominal yaw angle  $\psi_n$  due to its maximum rotation rate of

$0.20^\circ/\text{s}$  (Kouba, 2009). GPS Block II/IIA spacecraft cannot keep up with the required yaw rate as soon as the  $\beta$ -angle is smaller than  $3.6\text{--}4.9^\circ$  since their maximum rotation rates are limited to  $0.10\text{--}0.13^\circ/\text{s}$ . Moreover, when a GPS satellite enters the Earth's shadow, its solar sensors can no longer control the yaw-attitude due to the absence of the sunlight. Whereas the satellites from the Block IIR generation are basically able to keep their nominal attitude even in the dark (apart from the fact that the yaw angle is temporarily lagging behind  $\psi_n$  due to the insufficient hardware yaw rate), the Block II/IIA spacecraft start “yawing” with maximum hardware yaw rate as soon as they have entered the Earth's shadow. The rotation takes place in a predictable direction thanks to a permanent positive yaw bias implemented into the ACS by the US Air Force in the mid-1990's (Bar-Sever, 1994, 1996).

A first insight into the yaw-attitude behavior of the recently launched GPS Block IIF-1 satellite, also referred to as SVN62/PRN25, during eclipse season is given in Dilssner (2010).

#### 2.4.2. GLONASS satellites

GLONASS satellites have to meet the same requirements in terms of attitude control (i.e. Sun–Earth-pointing) as GPS satellites. For this purpose, the modernized generation of GLONASS-M spacecraft is equipped with ACS units promising accuracies for the nominal orientation of the BFS of  $0.5^\circ$  ( $x$ -axis),  $2.0^\circ$  ( $y$ -axis) and  $0.5^\circ$  ( $z$ -axis) (Bartenev et al., 2006). The solar panel's orientation of the first generation of GLONASS spacecraft, however, is regarded as uncertain during the Earth's shadow passage (Revnivykh and Mitrikas, 1998). Moreover, it is well-known that towards the end of their design life the old GLONASS satellites were switched off quite frequently during eclipsing periods, whereas the GLONASS-M spacecraft continue operating during eclipse even at advanced age (Dach et al., 2009). The sole exception is space vehicle number (SVN) 701, the second-oldest GLONASS-M satellite, which apparently is turned off by the system operators at the point where it is entering the Earth's penumbra and turned on again shortly after emerging from the penumbra.

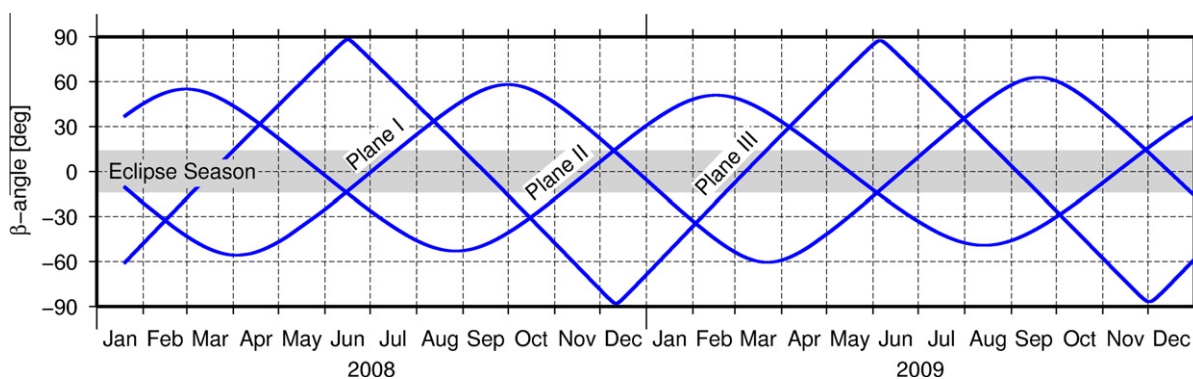


Fig. 2. Evolution of the elevation  $\beta$  of the Sun with respect to the three GLONASS orbital planes, viewed over two years (from January 2008 until December 2009).

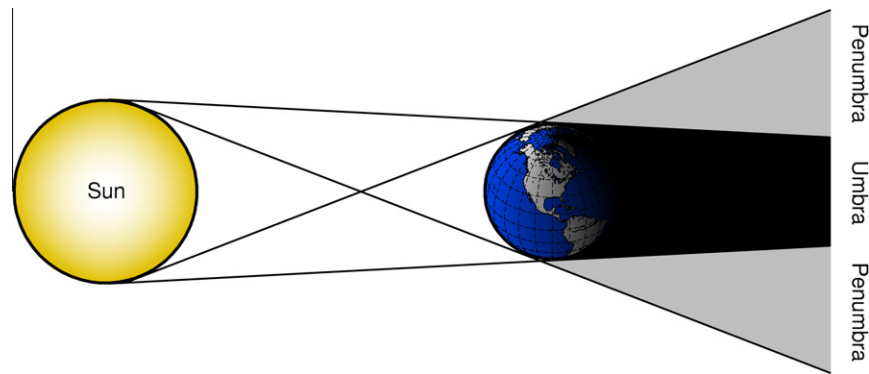


Fig. 3. Umbra and penumbra of the Earth's shadow.

The existing GNSS software packages having GLONASS processing capabilities, however, simply employ the nominal yaw-attitude model at all times, including during all the eclipse periods. This raises the vital question of how the GLONASS-M ACS actually controls the satellite's attitude in the absence of the sunlight and if the Russian space vehicles exhibit similar noon-turn and midnight-turn problems due to limited hardware yaw rates as their US-American competitors. There are indications that the GLONASS-M satellites are steered by a certain “eclipse passing algorithm” (Revnivykh, 2006). In the subsequent sections, we will shed some light on what is behind this algorithm.

### 3. Processing strategy

In order to study the actual yaw-attitude behavior of the GLONASS-M satellites during eclipse seasons, we have estimated their horizontal antenna phase center offset components epoch-by-epoch using 30-second observation data from a globally well-distributed set of multi-GNSS tracking stations. The number of stations observing a certain GLONASS-M spacecraft simultaneously or more specifically, contributing to the PCOs estimates, is 22 on average and varies by  $\pm 10$  (standard deviation, 1-sigma). The majority of stations belongs to the ground network of the International GNSS Service (IGS; Dow et al., 2009). In order to improve the global coverage, particularly in terms of the station density over North America, GPS/GLONASS data of 14 non-IGS sites from the GNSS Data Center of the Federal Agency for Cartography and Geodesy (BKG, Frankfurt/Main, Germany; <ftp://igs.bkg.bund.de/>) have been incorporated into our multi-GNSS analysis (Fig. 4).

The following 17 satellites of the GLONASS-M fleet – sorted by ascending SVNs – have been analyzed: 712 (R07), 713 (R24), 714 (R23), 715 (R14), 716 (R15), 717 (R10), 718 (R17), 719 (R20), 720 (R19), 721 (R13), 723 (R11), 724 (R18), 725 (R21), 726 (R22), 727 (R03), 728 (R02), 729 (R08). The attitude behavior of the latest set of six GLONASS-M satellites (SVN 730–735) operational since the beginning of 2010 has not been investigated as the particular orbital planes were not yet eclipsing.

As usual, we process dual-frequency code and phase measurements linearly combined to eliminate the first-order effect of ionospheric refraction. The satellite antenna PCOs are determined together with other geodetic parameters usually set up in global multi-GNSS analyses. To these belong: orbit parameters, Earth rotation parameters, troposphere parameters, clock parameters, inter-frequency biases, carrier phase ambiguities and station coordinates. However, due to the high mathematical correlations among PCOs and certain orbital elements, estimating all parameters in one run is a delicate issue. We therefore decided to keep the PCOs fixed to their nominal values for the time being and solve for the remaining GNSS parameters first. Afterwards, we estimate the satellite clock and antenna phase center positions epoch-by-epoch (with respect to the a priori orbit trajectory) whilst keeping all other parameters fixed. The processing scheme can be considered as a “reversed kinematic precise point positioning”. The nominal yaw-attitude standard model given by Eq. (1) thereby serves as an initial yaw-attitude model and provides the a priori yaw angle  $\psi_0(t)$  arising in Eq. (10). The estimated horizontal PCOs  $x_0(t)$  and  $y_0(t)$  are substituted into Eq. (8) in order to reveal the yaw bias  $\Delta\psi(t)$  existing between nominal and actual yaw angle. Estimates for the actual yaw angle  $\psi(t)$  are finally computed according to Eq. (10).

### 4. The GLONASS-M yaw-attitude maneuvers

#### 4.1. The shadow-crossing maneuver

The evolution of the estimated and the nominal yaw angle of SVN 724 during its passage through the Earth's shadow is depicted in Fig. 5. Before entering the shadow, the estimated and the nominal yaw angles are nearly identical. However, as soon as the satellite enters the umbra of the Earth ( $\epsilon_0 = -14.20^\circ$ ), we notice a linear drift in the estimated yaw angle. The spacecraft is now spinning around its body-fixed  $z$ -axis with maximum rotation rate. The sense of rotation is equivalent to the direction of the nominal yaw-attitude turn. The slope of a straight line fit yields yaw rates of  $0.24$ – $0.26^\circ/\text{s}$ . For  $\beta = 0^\circ$ , the satellite is yawing with

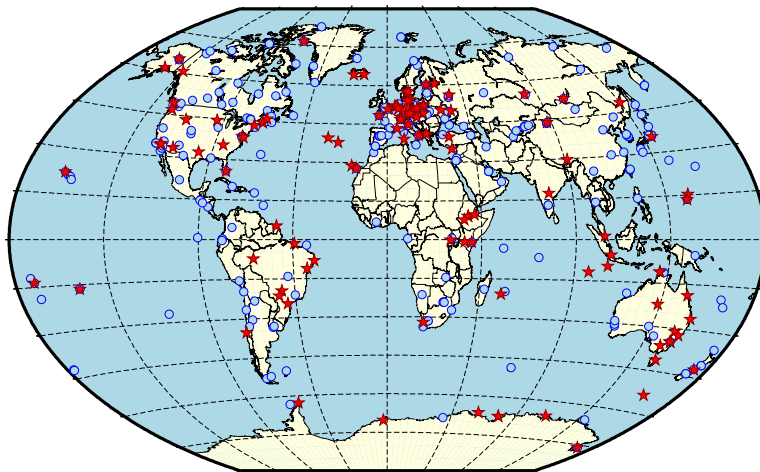


Fig. 4. Geographical overview of the 227 GPS-only (blue circles) and 115 GPS/GLONASS (red stars) ground stations used for this study. (For interpretation of the references to colour in this figure legend, the reader is referred to the web version of this article.)

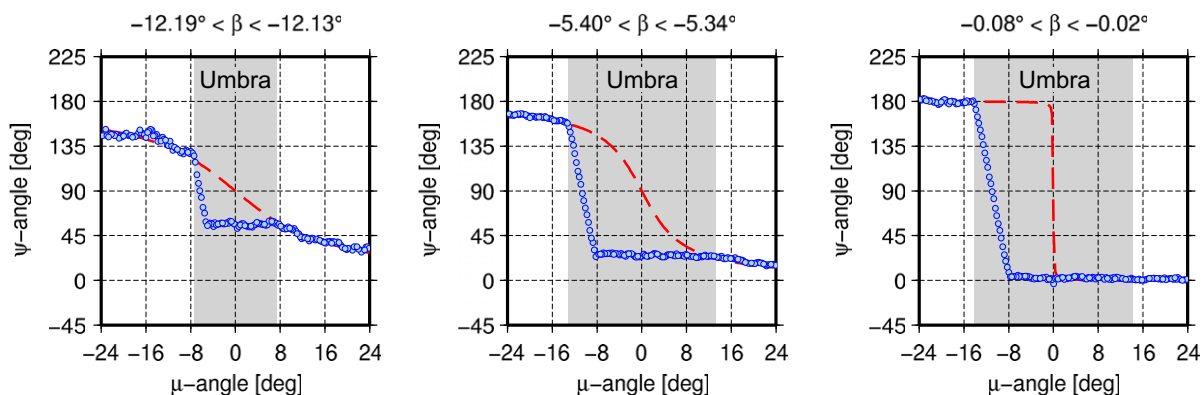


Fig. 5. Estimated and nominal yaw angles of SVN 724 crossing the Earth's shadow under different  $\beta$ -angles. The red dashed curves show the yaw angles assuming the midnight-turn maneuver is performed "nominally". The estimated yaw angle values are displayed as blue circles. They expose the actual yaw-attitude behavior of the GLONASS-M spacecraft during the eclipse phase. (For interpretation of the references to colour in this figure legend, the reader is referred to the web version of this article.)

maximum rate for about 12 min to perform a complete half turn. As soon as the actual yaw angle equals the nominal yaw angle to be expected at the end of the umbra ( $\epsilon_0 = +14.20^\circ$ ), the yaw-attitude is kept fixed (unlike a GPS Block II/IIA satellite which is continuously yawing during the entire eclipse phase and for up to 30 min beyond). When emerging from the Earth's shadow, the spacecraft is properly oriented again.

The nominal yaw-attitude turn markedly differs from the satellite's actual yaw-attitude behavior (cf. Fig. 5). Considering again the case of a sharp midnight-turn ( $\beta = 0^\circ$ ), the yaw-flip is supposed to take place up to 26.5 min later when the spacecraft approaches orbit midnight ( $\mu = 0^\circ$ ). During this time, the actual yaw-attitude differs from the nominal by up to  $\pm 180^\circ$ . Neglecting a yaw bias in this order of magnitude has a tremendous negative impact on the satellite antenna phase center correction as we will demonstrate later.

It is worth mentioning at this point that almost all the other GLONASS-M space vehicles we have analyzed are

following this yaw-attitude scheme during eclipse, except for SVN 713. The estimated yaw angles of SVN 713 have shown that the satellite more or less keeps its nominal yaw-attitude even in the Earth's shadow. In this respect, SVN 713 basically behaves like a GPS Block IIR satellite. Independent sources have informed us that the solar sensors on-board of SVN 713 are malfunctioning. How the spacecraft determines its yaw-attitude in the absence of properly functioning sun sensors remains unclear. SVN 713 was decommissioned in February 2010.

#### 4.2. The noon-turn maneuver

The GLONASS-M noon-turn maneuver is expected to be much shorter and thus less critical than the shadow-crossing maneuver. It should only occur if the elevation  $\beta$  of the Sun drops below a relatively small angle  $\beta_0$ . Since we know the mean orbital angular velocity  $\dot{\mu}_0$  and determined the maximum yaw rate of the GLONASS-M spacecraft to be  $0.24\text{--}0.26^\circ/\text{s}$ , computing the threshold value  $\beta_0$

for the noon-turn maneuver is straightforward (see Kouba, 2009). Substituting  $\dot{\psi}_n = 0.25^\circ/\text{s}$ ,  $\mu = 180^\circ$  and  $\dot{\mu}_0 = 0.00888^\circ/\text{s}$  in Eq. (2) and solving for  $\beta$  yields  $\beta_0 = 2.0^\circ$ . This means that only satellites with  $|\beta| < 2.0^\circ$  will experience a noon-turn maneuver.

The evolution of the estimated and the nominal yaw angle of SVN 724 passing the region around orbit noon under slightly different small  $\beta$ -angles is illustrated in Fig. 6. Again we notice that the satellite is spinning around its body-fixed  $z$ -axis with a nearly constant yaw rate of around  $0.24\text{--}0.26^\circ/\text{s}$  in order to accomplish the required yaw-flip. We actually would have expected the noon-turn maneuver not to be started until the required nominal yaw rate exceeds the actual spacecraft's yaw angle, but this appears not to be the case. In fact, the spacecraft starts yawing at full rate a little earlier already so that the actual yaw angle at the orbit's noon point ( $\mu = 180^\circ$ ) is  $\pm 90^\circ$ . This keeps the maximum deviation between actual and nominal yaw angle throughout the maneuver as small as possible and thus reduces the impact on the user.

For  $\beta = 0^\circ$ , the noon-turn maneuver lasts approximately 12 min and the actual and the nominal yaw angle differ by up to  $\pm 90^\circ$ . This may cause a range error in the satellite antenna phase center correction of up to  $\pm 19.0$  cm. For  $\beta \neq 0^\circ$ , the maneuver is shorter and the maximum yaw bias smaller.

## 5. The GLONASS-M yaw-attitude model

### 5.1. Modeling the shadow-crossing maneuver

As we have learned from the study of the estimated yaw angles, the GLONASS-M shadow-crossing maneuver immediately starts after the spacecraft has entered the beginning of the umbra. The orbital angles  $\mu_s$  and  $\mu_e$  upon shadow entry and shadow exit, respectively, can be calculated as follows:

$$\mu_e = -\mu_s = \arccos(\cos \epsilon_0 / \cos \beta). \quad (11)$$

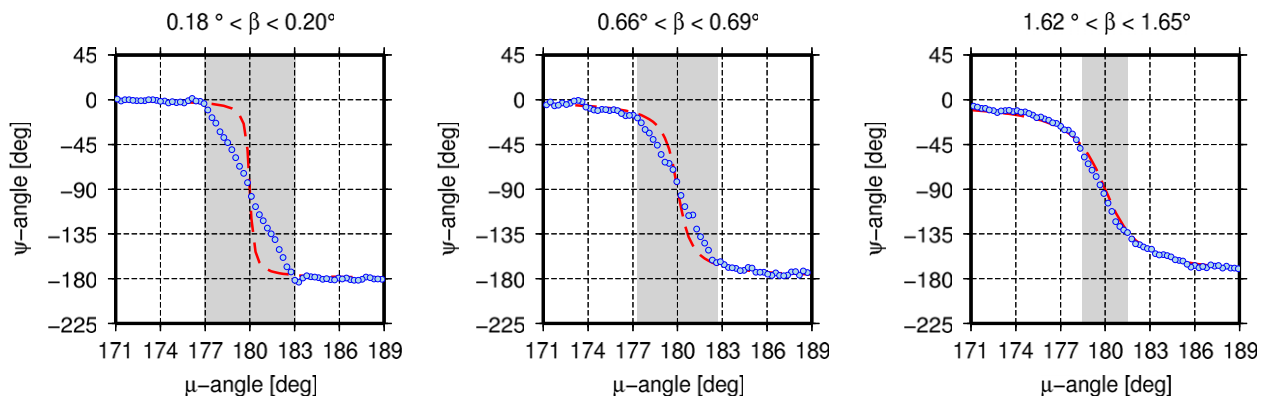


Fig. 6. Estimated and nominal yaw angles of SVN 724 passing the region around orbit noon under different  $\beta$ -angles. The shaded areas illustrate the duration of the noon-turn regime. The red dashed curves show the yaw angles assuming the  $180^\circ$  noon-turn maneuver is performed “nominally”. The estimated yaw angle values are displayed as blue circles. They reveal the actual yaw-attitude behavior of the GLONASS-M spacecraft during orbit noon. (For interpretation of the references to colour in this figure legend, the reader is referred to the web version of this article.)

The sign of the actual yaw rate during the midnight-turn is the same as the sign of the nominal yaw rate  $\dot{\psi}_n(\mu_s)$  at shadow entry. Neglecting the acceleration that is needed for the spacecraft to reach its maximum yaw rate, the yaw angle during the entire shadow crossing period can be described as follows:

$$\psi(\mu) = \text{ATAN2}(-\tan \beta, \sin \mu_s) + \text{SIGN}[R, \dot{\psi}_n(\mu_s)] \cdot (\mu - \mu_s) / \dot{\mu} \quad (12)$$

for  $\mu_s < \mu < \mu_f$  and

$$\psi = \text{ATAN2}(-\tan \beta, \sin \mu_e) \quad (13)$$

for  $\mu_f < \mu < \mu_e$ .  $\text{SIGN}(a, b)$  is the usual FORTRAN function returning the value of  $a$  with the sign of  $b$ .  $R$  denotes the hardware yaw rate.

The orbital angle  $\mu_f$  defines the position within the Earth's shadow where the actual yaw angle has reached the nominal yaw angle  $\psi_n(\mu_e)$  upon shadow exit and the spacecraft switches into fixed-yaw mode. From the intersection of lines defined by Eqs. (12) and (13) we obtain:

$$\mu_f = \{ \dot{\mu} [\text{ATAN2}(-\tan \beta, \sin \mu_e) - \text{ATAN2}(-\tan \beta, \sin \mu_s)] / \text{SIGN}[R, \dot{\psi}_n(\mu_s)] \} + \mu_s. \quad (14)$$

The orbital angle  $\mu_f$  essentially depends on the size of the  $\beta$ -angle. At the beginning as well as at the end of the eclipse season ( $\beta = \pm 14.2^\circ$ ),  $\mu_f$  equals  $0^\circ$ . The angle increases as the  $\beta$ -angle decreases. For a deep shadow eclipse ( $\beta = 0^\circ$ ), we obtain  $\mu_f = -7.8^\circ$  (cf. Fig. 5).

### 5.2. Modeling the noon-turn maneuver

The yaw angle during the noon-turn maneuver can formally be described like the shadow-crossing maneuver:

$$\psi(\mu) = \text{ATAN2}(-\tan \beta, \sin \mu_s) + \text{SIGN}[R, \dot{\psi}_n(\mu_s)] \cdot (\mu - \mu_s) / \dot{\mu}, \quad (15)$$

with  $\mu_s$  as the orbital angle defining the beginning of the maneuver. From Fig. 6 we may conclude that the orbital angles  $\mu_s$  and  $\mu_e$  at the start and the end of the maneuver satisfy the following relationship:

$$\pi - \mu_s = \mu_e - \pi. \quad (16)$$

We will now derive the orbital angle  $\mu_s$ . In order to avoid needlessly complicated notations we focus on the case  $\psi_n(\mu_s) < 0$  along with the small angle approximation of  $\tan\beta \approx \beta$ . Thus what we need to find now is the intersection point between the straight line

$$\psi(\mu) = R \cdot (\pi - \mu) / \dot{\mu} - \pi/2 \quad (17)$$

and the nominal yaw curve

$$\psi_n(\mu) = -\arctan(|\beta| / \sin \mu). \quad (18)$$

To overcome the non-linearity of Eq. (18), we approximate the function by a first-order Taylor series expansion about the point  $\mu = \mu_0$  and obtain:

$$\psi_n(\mu) \approx -\arctan(|\beta| / \sin \mu_0) - |\beta| \cos \mu_0 (\mu - \mu_0) / (\beta^2 + \sin^2 \mu_0). \quad (19)$$

The orbital angle  $\mu_s$  is then found from the intersection of the lines defined by Eqs. (17) and (19):

$$\mu_s = \left[ \arctan(|\beta| / \sin \mu_0) + |\beta| \cos \mu_0 / (\beta^2 + \sin^2 \mu_0) + \pi R / \dot{\mu} - \pi/2 \right] / [R / \dot{\mu} + |\beta| \cos \mu_0 / (\beta^2 + \sin^2 \mu_0)]. \quad (20)$$

For  $\beta = 0^\circ$ , we directly obtain  $\mu_s = 176.8^\circ$ . For  $\beta \neq 0^\circ$ , the equation has to be solved iteratively whereas  $\mu_0 = 176.8^\circ$  has proven to be a reasonable value for the initial run. To ensure adequate precision for every possible noon-turn maneuver scenario ( $0^\circ < |\beta| < 2.0^\circ$ ), four iterations are recommended. The orbital angle  $\mu_e$  then follows from Eq. (16):

$$\mu_e = 2\pi - \mu_s. \quad (21)$$

## 6. Performance validation

### 6.1. Implementation aspects

The yaw-attitude model for the GLONASS-M shadow-crossing and noon-turn maneuver outlined in the previous sections has been implemented into our multi-GNSS analysis software, the Navigation Package for Earth Observation Satellites (NAPEOS; Springer, 2009). For the sake of simplicity, we have used an average hardware yaw rate of  $R = 0.25^\circ/s$  for all satellites. Since the individual maximum yaw rate may deviate from this mean value by up to  $\pm 0.01^\circ/s$ , we have to reckon with remaining yaw-attitude errors. A yaw rate error of  $\pm 0.01^\circ/s$  can cause a yaw-attitude error at the end of a 12-minute duration half-turn of about  $\pm 7^\circ$ .

### 6.2. Impact on phase residuals and satellite clocks

For validation purposes, we have reprocessed the 30-second satellite clock solutions, however, now without

solving for the satellite antenna offset parameters anymore. The estimation strategy therefore corresponds to the processing scheme currently employed at ESA/ESOC for the routine generation of our high-rate IGS final clock product. Errors arising from the mismodeling of the satellite antenna phase center due to an erroneous yaw angle during orbit noon and orbit midnight should now propagate into the carrier phase and pseudo-range residuals. When employing the nominal yaw-attitude model, we actually notice a considerable increase of the ionosphere-free phase residuals during Earth shadow-crossing (Fig. 7). Depending on the azimuth and the nadir-angle under which a particular ground station is seen from a GLONASS-M satellite, the effect may reach up to  $\pm 27$  cm. The error contribution due to the mismodeling of the phase wind-up effect is not reflected in the residuals, as it has been absorbed by the satellite clock parameters.

The results clearly underline that the GLONASS-M satellites do require a special yaw-attitude modeling during eclipse because phase errors on decimeter-level are unacceptable as they are generally causing the respective observations to be excluded from further processing which, in turn, may considerably weaken epoch-dependent parameters like satellite clocks or “kinematic” stations coordinates. In order to quantify how much information during eclipse might actually get lost and therefore does not contribute to the satellite clock estimates, we accumulated the number of non-rejected ground stations per satellite and epoch. Fig. 8 depicts, satellite-wise, the drastic decrease in the number of stations satisfying the outlier test criteria when the nominal yaw-attitude model is used. We notice that the number drops almost down to zero, which is equivalent to a significant loss of precision of the satellite clock estimates. Indeed, in some cases *all* ground stations observing an eclipsing satellite at a certain epoch are rejected, which then makes the satellite clock solution impossible.

A more realistic modeling of the satellite’s yaw-attitude should prevent the observation residuals from being increased during eclipse seasons. We actually notice that when employing the new GLONASS-M yaw-attitude model the magnitude of the phase residuals inside and outside the Earth’s shadow is consistently on the same level (cf. Fig. 7). This means that we do not have to be concerned about the associated observations being incorrectly identified as outliers and getting rejected (cf. Fig. 8). The same holds for the measurements made during the period around orbit noon.

The reduction of the carrier phase residuals when using the new yaw-attitude model should also manifests itself in the RMS statistics of our daily IGS solutions. Usually, the daily phase RMS values for eclipsing GLONASS-M satellites are about 10% higher compared to the RMS values of non-eclipsing GLONASS-M satellites. A reprocessing of our IGS final orbit and clock solutions from the years 2008/2009 using the new yaw-attitude model demonstrates that we are now capable of reducing the daily phase RMS values during eclipse seasons down to the normal

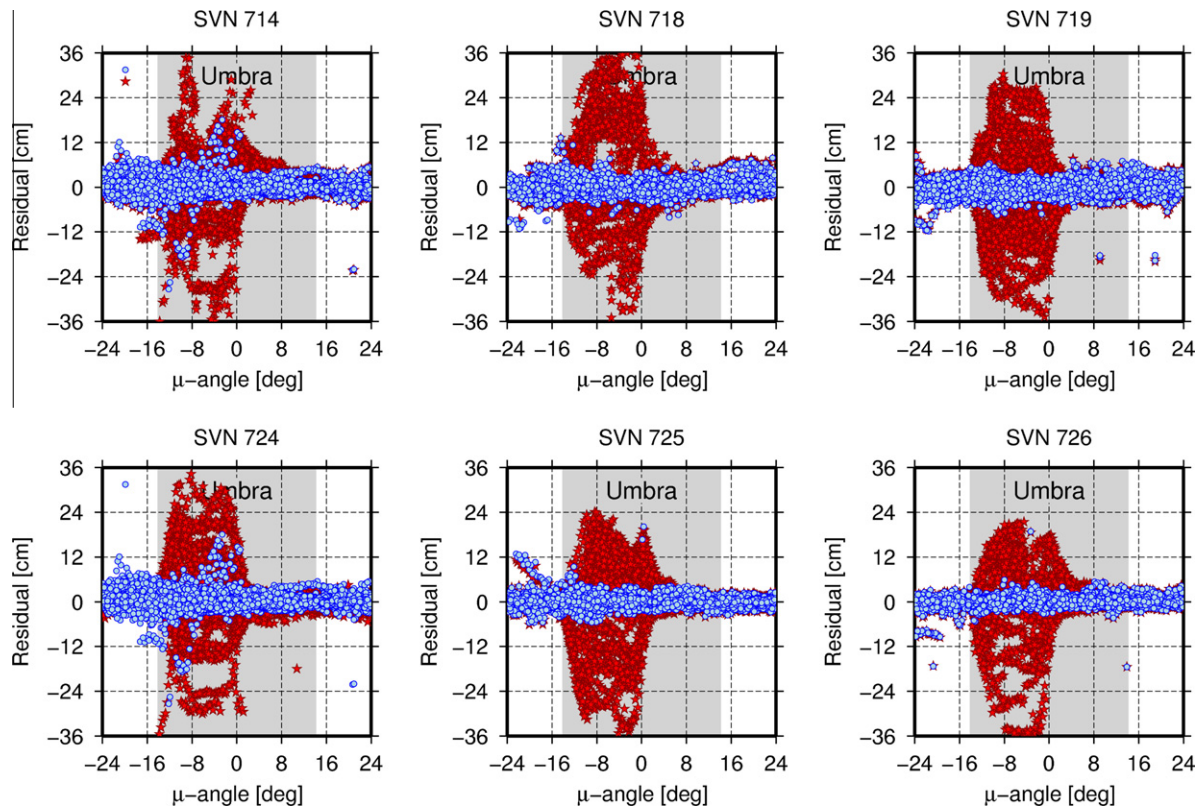


Fig. 7. Ionosphere-free observation residuals for the carrier phase measurements between all GLONASS-capable ground stations and six GLONASS-M satellites during a deep eclipse ( $\beta \approx 0^\circ$ ) of orbital plane number III on March 9, 2009. The residuals associated with the nominal yaw-attitude model are displayed as red stars. The blue circle symbols show the residuals obtained with the new yaw-attitude model. (For interpretation of the references to colour in this figure legend, the reader is referred to the web version of this article.)

level outside of the eclipse season (Fig. 9). The improvement of the RMS statistics goes along with an increased number of observations per day (around 2.5% in average) now passing the NAPEOS outlier detection.

### 6.3. Impact on precise point positioning

In this section we investigate how the accuracy of precise point positioning (PPP) of ground sites may degrade in case of a GLONASS orbital plane being partially eclipsed. We focus on kinematic PPP as the strongest impact of an incorrect yaw-attitude can be expected when station coordinates, along with tropospheric zenith path delays (ZPDs), are estimated epoch-wise (Kouba, 2009). Since the vast majority of GLONASS users today performs combined GPS/GLONASS data processing to take advantage of the increased availability of GNSS satellites, we restrict our analysis to combined GPS/GLONASS PPP. Consistent satellite orbits and clocks are adopted from the global network solutions described previously.

We found that using the nominal yaw-attitude standard model for the GLONASS-M satellites during eclipse seasons may seriously affect the coordinate solutions. This has been evident, for instance, in the results obtained for the IGS station “MAL2” at Malindi, Kenya. The measurement data used in this example were collected on March 9,

2009, when four out of 18 GLONASS-M satellites being tracked by the station were passing through the entire Earth’s shadow. The total number of usable GNSS satellites per epoch ranges from 11 to 19 and the PDOP (“Position Dilution of Precision”) value varies between one and two indicating a strong observation geometry throughout the day. The average 3D position error (RMS) outside the eclipse intervals is around  $\pm 3$  cm. However, after the entrance of SVN 726 and SVN 714 into the Earth’s umbra at around 20:10 and 21:36 UTC, respectively, we notice an increasing degradation of the positioning accuracy, particularly in the height component, in the order of a few decimeters when employing the nominal yaw-attitude standard model (Fig. 10). The reason for this considerable impact is related to the high mathematical correlations among the epoch-dependent station parameters (height, clock, tropospheric ZPD) and the poor outlier resistance capabilities of the least-squares adjustment process, as a closer look on an affected single-epoch solution reveals: Instead of detecting and rejecting them, the erroneous observations belonging to the eclipsing satellite remain undetected in the equation system and thus falsify the parameters to be estimated. This, in turn, increases the residuals of other (non-eclipsing) satellites belonging to the same epoch and may cause the outlier detection to reject those observations. During the shadow-crossing

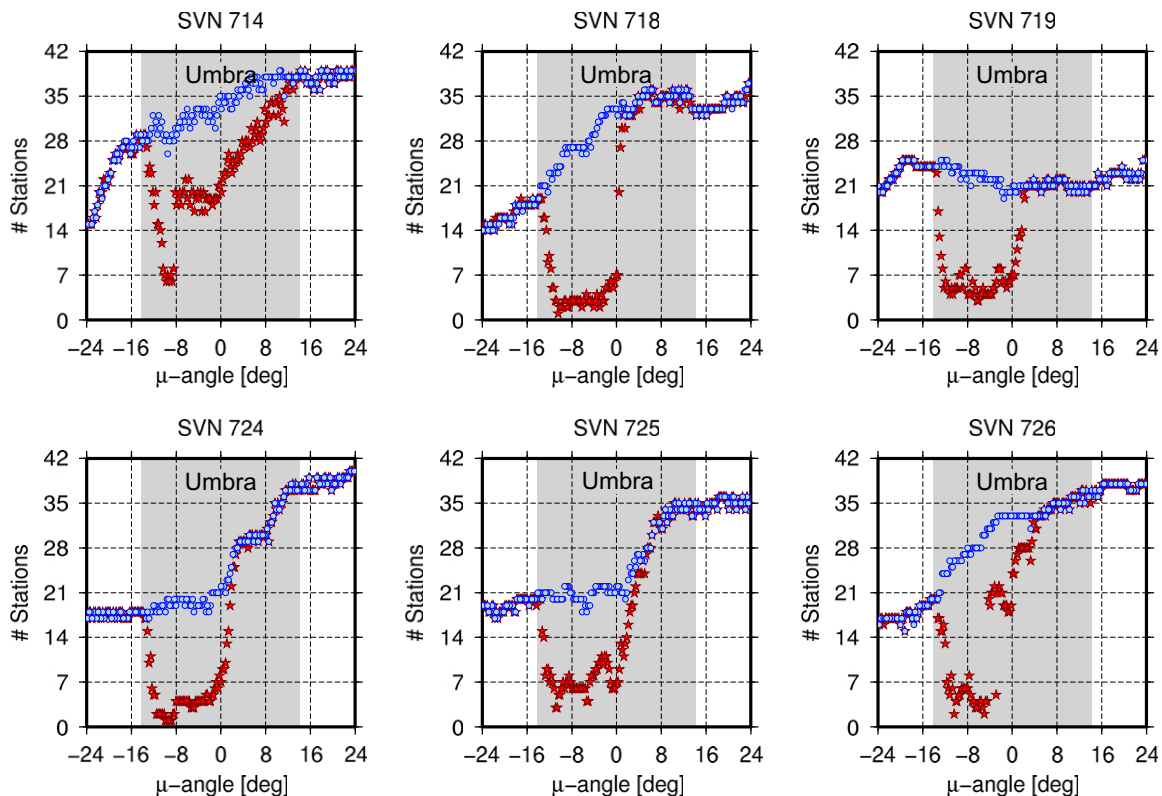


Fig. 8. Number of ground stations satisfying the outlier test criteria during a deep eclipse ( $\beta \approx 0^\circ$ ) of orbital plane number III on March 9, 2009. The values obtained with the nominal yaw-attitude model are illustrated as *red stars*. The *blue circle* symbols show the values obtained with the new yaw-attitude model. (For interpretation of the references to colour in this figure legend, the reader is referred to the web version of this article.)

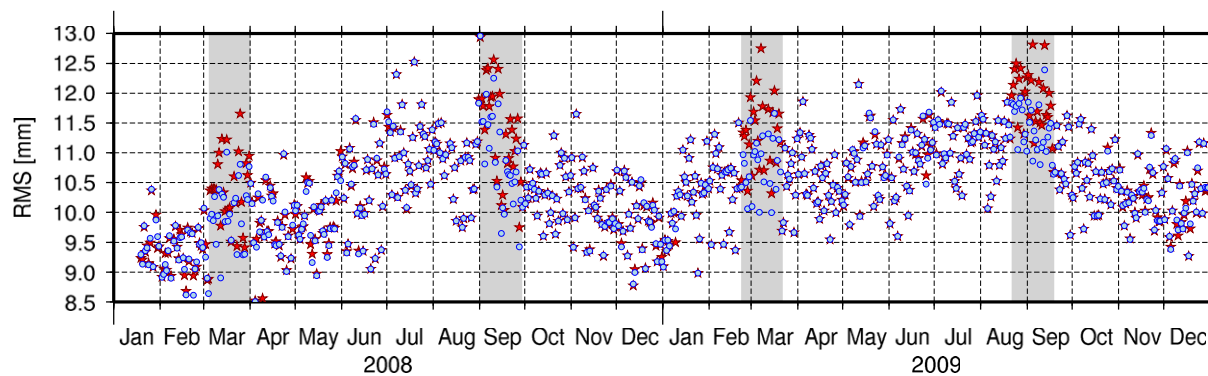


Fig. 9. Daily phase RMS statistics of SVN 719 from January 2008 until December 2009. The *shaded* areas indicate the eclipse seasons. The RMS values obtained with the nominal yaw-attitude model are illustrated as *red stars*. The *blue circle* symbols show the RMS values obtained with the new yaw-attitude model. (For interpretation of the references to colour in this figure legend, the reader is referred to the web version of this article.)

maneuvers of SVN 719 and SVN 725, the outlier detection worked well as solely the particular eclipsing satellite was excluded from the solution. Thanks to the still large number of well-distributed GPS and GLONASS satellites, the absence of SVN 719 and SVN 725 has hardly any negative effect on the positioning accuracy (cf. Fig. 10). In the case of the shadow-crossing maneuvers of SVN 726 and SVN 714, however, the actual outliers caused by the wrong yaw-attitude modeling of the two particular satellites remained undetected. Besides this, the (unbiased) observations of two more GPS satellites were excluded.

In the worst case, the number of satellites satisfying the outlier test criteria drops below the minimum number needed for fixing a position. In the kinematic PPP analysis of the IGS station “MOBS” (Melbourne, Australia) using again GPS/GLONASS data from March 9, 2009, for instance, we detected 10 epochs which could not be solved at all since the associated observations were completely rejected. The reason for this could be found again in the wrong yaw-attitude modeling of SVN 714 when passing through the Earth’s shadow. The problem did not arise when the new GLONASS-M yaw-attitude model was used.

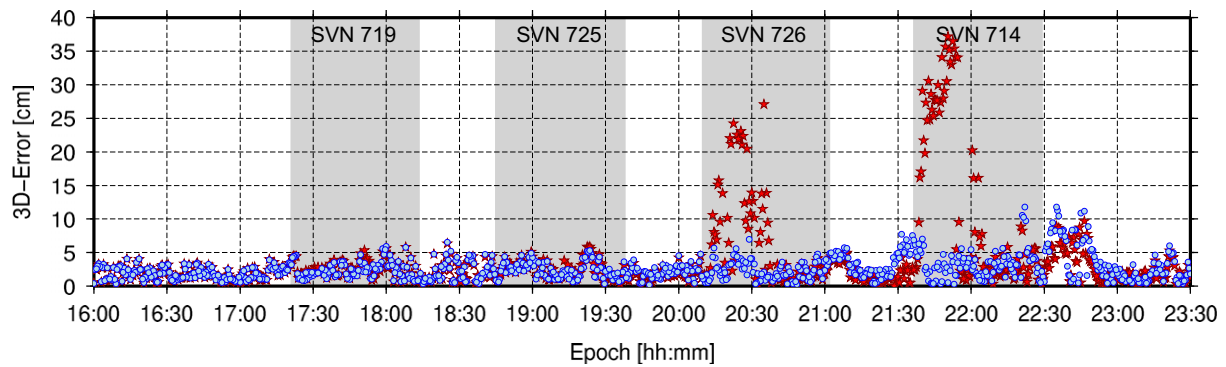


Fig. 10. Positioning errors of kinematic PPP solutions for the IGS station MAL2 using GPS/GLONASS data from March 9, 2009. The shaded areas indicate the shadow passages of four GLONASS-M satellites. The errors obtained with the nominal yaw-attitude model are illustrated as red stars. The blue circle symbols show the errors obtained with the new yaw-attitude model. (For interpretation of the references to colour in this figure legend, the reader is referred to the web version of this article.)

## 7. Summary and conclusions

We have demonstrated that the existence of a horizontal GNSS satellite antenna phase center eccentricity can be exploited to derive the spacecraft's yaw-attitude. The method has been successfully applied to investigate the yaw-attitude behavior of GLONASS-M satellites traveling in eclipsing orbits around the Earth. We found that as soon as the satellites enter into the umbra of the Earth's shadow, they start spinning around their body-fixed  $z$ -axis with rotation rates in the range of  $0.24$ – $0.26^\circ/\text{s}$ . Unlike GPS Block II/IIA satellites, which rotate permanently with maximum speed during the entire shadow phase and beyond, GLONASS-M spacecraft switch into a fixed-yaw mode as soon as they have completed their required midnight-turn, that is, after a maximum of 12 min. In this way, they are properly oriented when emerging from the Earth's shadow and returning into sunlight. During the eclipse phase, however, the actual yaw-attitude may deviate from the nominal by up to  $\pm 180^\circ$ . This causes range errors in the satellite antenna phase center correction of up to  $\pm 27$  cm as a close inspection of the phase observation residuals has revealed. Whenever the elevation  $\beta$  of the Sun is below  $2.0^\circ$  and a GLONASS-M satellite approaches the region around orbit noon, it cannot keep up anymore with the rapidly changing nominal yaw angle due to its limited hardware rotation rate. The noon-turn maneuver is less critical than the shadow-crossing maneuver as it may last up to 12 min at most and the maximum yaw bias is limited to  $\pm 90^\circ$ . The resulting range error due to the mismodeling of the satellite antenna phase center correction during orbit noon may amount to  $\pm 19$  cm. Besides this, dynamic orbit errors due to erroneous modeling of the solar pressure effects around noon can be expected since the spacecraft is in full sunlight now.

There is evidence to suggest that the next-generation of GLONASS spacecraft, GLONASS-K, will have significantly smaller or even no attitude-related antenna phase center modeling issues during eclipse seasons as they apparently exhibit much smaller horizontal antenna phase

center eccentricities than the satellites from the M series (Dilssner et al., 2010). More precise statements on this can be made after the launch of the first GLONASS-K satellite, which is scheduled for December 2010.

The GLONASS-M shadow-crossing and noon-turn maneuver can be accurately modeled by using a constant hardware yaw rate of  $0.25^\circ/\text{s}$ . It has been clearly shown that a proper yaw-attitude model as outlined in this paper reduces the phase observation residuals during eclipse seasons down to the normal level outside of the eclipse season and that a single eclipsing GLONASS-M satellite may degrade the positioning accuracy in kinematic PPP applications in the order of a few decimeters if its yaw-attitude is mismodeled. Future studies are needed to assess whether it is worthwhile to use satellite-specific yaw rates or if a block-specific mean value applied to all GLONASS-M spacecraft is entirely sufficient. The usage of satellite-specific yaw rates would then bring up the question whether these rates should be treated as constant or time-dependent parameters which have to be estimated routinely.

In addition to the benefits a proper yaw-attitude modeling provides for the GNSS measurements, the new model should also help to improve the results of GLONASS-M satellite laser ranging (SLR) during eclipse as the center of the laser retroreflector array (LRA) carried by each GLONASS-M spacecraft also exhibits a significant horizontal offset ( $\tilde{x}_0 = 13.7$  cm,  $\tilde{y}_0 = 0.3$  cm) with respect to the CM (ILRS satellite parameters, 2010). Even though the center of the LRA is located four times closer to the satellite's  $z$ -axis than the mean phase center of the GNSS microwave antenna, a wrong yaw-attitude may significantly falsify the LRA offset correction. Depending on the azimuth and the nadir-angle under which a particular SLR tracking station is seen from a GLONASS-M satellite, the effect may theoretically reach up to  $\pm 7$  cm.

## Acknowledgments

The authors gratefully acknowledge IGS and BKG for providing global GNSS data and ephemerides. We also

extend our thanks to John B. Palmer from Logica for his valuable comments on the manuscript and the NAPEOS development team at ESA/ESOC without whose support the software would not have attained such a high level of performance.

## References

- Bar-Sever, Y. New GPS attitude model, in: IGSMail-0591. IGS Central Bureau, Pasadena, 1994.
- Bar-Sever, Y. A new model for GPS yaw attitude. *J. Geod.* 70 (11), 714–723, doi:10.1007/BF00867149, 1996.
- Bartenev, V., Kosenko, V., Chebotarev, V. Builders notes: Russian GLONASS at the stage of active implementation. InsideGNSS, April. Available at <<http://www.insidegnss.com/auto/0406%20Builders.pdf>>, 2006.
- Choi, C. Phase centers of GPS IIF modernization L-band antenna, in: Proceedings of the 15th International Technical Meeting of the Satellite Division of The Institute of Navigation (ION GPS 2002), Portland, OR, 24–27 September, pp. 241–244, 2002.
- Dach, R., Brockmann, E., Schaer, S., Beutler, G., Meindl, M., Prange, L., Bock, H., Jäggi, H., Ostini, L. GNSS processing at CODE: status report. *J. Geod.* 83 (3–4), 353–365, doi:10.1007/s00190-008-0281-2, 2009.
- Dilssner, F. GPS IIF-1 satellite antenna phase center and attitude modeling. InsideGNSS, September. Available at <<http://www.insidegnss.com/auto/sep10-Dilssner.pdf>>, 2010.
- Dilssner, F., Springer, T., Flohrer, C., Dow, J. Estimation of phase center corrections for GLONASS-M satellite antennas. *J. Geod.* 84 (8), 467–480, doi:10.1007/s00190-010-0381-7, 2010.
- Dow, J.M., Neilan, R.E., Rizos, C. The International GNSS Service in a changing landscape of global navigation satellite systems. *J. Geod.* 83 (7), 191–198, doi:10.1007/s00190-008-0300-3, 2009.
- ILRS satellite parameters. Available at: <[http://ilrs.gsfc.nasa.gov/satellite\\_missions/list\\_of\\_satellites](http://ilrs.gsfc.nasa.gov/satellite_missions/list_of_satellites)>, 2010.
- Kouba, J. A simplified yaw-attitude model for eclipsing GPS satellites. *GPS Solut.* 13 (1), 1–12, doi:10.1007/s10291-008-0092-1, 2009.
- Mitrikas, V. GLONASS-M dimensions and center-of-mass correction, in: IGSMail-5104. IGS Central Bureau, Pasadena, 2005.
- Revnivykh, S. GLONASS: policy, status and modernization plan. Presented at Munich Satellite Navigation Summit, February 21–23. Available at: <[http://www.munich-satellite-navigation-summit.org/Summit2006/Beitraege/Ses\\_1\\_4\\_Revnivykh.pdf](http://www.munich-satellite-navigation-summit.org/Summit2006/Beitraege/Ses_1_4_Revnivykh.pdf)>, 2006.
- Revnivykh, S., Mitrikas, V. GLONASS S/C mass and dimension, in: IGEXMail-0086. IGS Central Bureau, Pasadena, 1998.
- Rothacher, M., Schmid, R. ANTEX: The antenna exchange format version 1.3. Format specifications, IGS Central Bureau, Pasadena. Available at: <<ftp://igs.org/igs/scb/station/general/antex13.txt>>, 2006.
- Springer, T.A. NAPEOS mathematical models and algorithms. Technical note, DOPS-SYS-TN-0100-OPS-GN. Available at: <<ftp://dgn6.eso-c.esa.int/cool/DOPS-SYS-TN-0100-OPS-GN-MathModels.pdf>>, 2009.
- Wu, J.T., Wu, S.C., Hajj, G.A., Bertiger, W.I., Lichten, S.M. Effects on antenna orientation on GPS carrier phase. *Manuscr Geod* 18 (2), 91–98, 1993.